Supporting Information for

Evolution of atmospheric age of particles and its implications for the formation of a severe haze event in eastern China

Xiaodong Xie[1], Jianlin Hu[1*], Momei Qin[1], Song Guo[2], Min Hu[2], Dongsheng Ji[3], Hongli

Wang[4], Shengrong Lou[4], Cheng Huang[4], Chong Liu[5], Hongliang Zhang[6], Qi Ying[7], Hong

Liao[1], Yuanhang Zhang[2]

[1] Jiangsu Key Laboratory of Atmospheric Environment Monitoring and Pollution Control,
Collaborative Innovation Center of Atmospheric Environment and Equipment Technology, Nanjing
University of Information Science & Technology, Nanjing 210044, China
[2] State Key Joint Laboratory of Environmental Simulation and Pollution Control, College of
Environmental Sciences and Engineering, Peking University, Beijing, 100871, China
[3] State Key Laboratory of Atmospheric Boundary Layer Physics and Atmospheric Chemistry, Institute
of Atmospheric Physics, Chinese Academy of Sciences, Beijing, 100191, China
[4] State Environmental Protection Key Laboratory of Formation and Prevention of Urban Air Pollution
Complex, Shanghai Academy of Environmental Sciences, Shanghai, 200233, China
[5] CMA Earth System Modeling and Prediction Centre, State Key Laboratory of Severe Weather, China
Meteorological Administration (CMA), Beijing 100081, China
[6] Department of Environmental Science and Engineering, Fudan University, Shanghai 200438, China
[7] Zachry Department of Civil Engineering, Texas A&M University, College Station, Texas 77843,
USA

Corresponding author: Jianlin Hu (jianlinhu@nuist.edu.cn)

Contents of this file

Text S1. Model evaluation

Evaluation of WRF-simulated meteorological parameters in the NCP and the YRD during this haze episode is shown in **Figure S1**. The corresponding mean bias (MB), mean error (ME), root mean square error (RMSE), correlation coefficient (R), and index of agreement (IOA) were calculated and summarized in **Table S1**. Compared with observations in both the NCP and the YRD, the WRF model captures well the magnitude and temporal variation of T2 and RH with high correlation coefficients of 0.97–0.98, but slightly underestimates T2 with MBs of −0.2 °C to −0.1 °C and overestimates RH with MBs of 0.5% to 2.6%. The simulated WS is underestimated with MBs of −0.35 m s^{-1} to −0.26 m s^{-1}, especially for high wind speed conditions. The RMSEs of WS are less than 1 m s^{-1} and the IOAs are larger than 0.7, which satisfy the benchmarks suggested by Emery et al. (2001). For WD, the MEs are less than 30° and the correlation coefficients are larger than 0.8, indicating the WRF model can capture the variations of wind direction during this haze episode. Overall, the simulated meteorological parameters in this study agree well with observations, and the model performance is comparable to other works using the WRF model in China (Chen et al., 2017a; Hu et al., 2016; Zheng et al., 2015a).

The UCD/CIT model performance of PM$_{2.5}$ and its major chemical compositions in eastern China is evaluated. The UCD/CIT model well reproduces the observed temporal variations of hourly PM$_{2.5}$ concentrations averaged over the NCP and the YRD during this haze episode with a high correlation coefficient (R > 0.85) and a low bias (NMB < 15%) (**Figure 3b**). High PM$_{2.5}$ concentrations (> 150 μg m^{-3}) with low wind speed over southern Hebei, Shandong, Henan, northern Jiangsu, and Anhui provinces are well captured by the model (**Figure S4**). The simulated PM$_{2.5}$ compositions (SO$_4^{2-}$, NO$_3^-$, NH$_4^+$, EC, and organic matter (OM)) also agree well with the daily-averaged measurements in Beijing, Jinan, Nanjing, and Shanghai (**Figure 2**), with model performance statistics comparable to those in other studies (Shi et al., 2017; Hu et al., 2016; Zhang et al., 2019b). The correlation coefficients of SO$_4^{2-}$, NO$_3^-$, and NH$_4^+$ are found to be 0.80, 0.80, and 0.87 respectively, indicating that the UCD/CIT model successfully captures the day-to-day variations of secondary inorganic aerosols (SO$_4^{2-}$, NO$_3^-$, and NH$_4^+$; hereafter referred to as SNA).

However, the model significantly underestimates SO_4^{2-} concentrations with an NMB of −42.3%, especially when the observed SO_4^{2-} concentrations are high. Underestimation of SO_4^{2-} has also been pointed out by many other modeling studies in China, which is mainly attributed to the missing mechanisms, such as heterogeneous chemistry, in current air quality models (Song et al., 2021; Zheng et al., 2015a; Wang et al., 2014). The model captures the observed NO_3^- concentrations well, with an NMB and NME of −7.8% and 33.1% respectively. The model performance of NH_4^+ is better than SO_4^{2-} but slightly worse than NO_3^-, and the NMB and NME values meet the performance criteria. The UCD/CIT model can generally capture the spatiotemporal variations of EC but has a positive NMB of 62.6%. The large overestimation of EC is mainly attributed to the uncertainties in emission inventory, which has also been found in previous studies (Zheng et al., 2015a; Wang et al., 2021d). Other reasons, such as the relatively coarse model grid resolution (36 km) and uncertainties in predicted meteorological parameters, may also contribute to this bias (Hu et al., 2016; Liu et al., 2020). The NMB and NME of OM meet the model performance criteria, indicating OM predictions agree well with measurements. Nevertheless, OM is slightly underestimated with an NMB of −6.3%. This is mainly attributed to the underestimations in SOA due to the missing formation pathways such as multigenerational aging of semi-volatile organic compounds, and heterogeneous and aqueous-phase pathways in current air quality models (Chen et al., 2017b; Hu et al., 2015).

Overall, the above evaluations suggest that the simulated meteorological parameters and particle concentrations are consistent with observations, verifying a good model performance in eastern China during this haze episode.

Table S1. Statistical evaluations of meteorological performance

	OBS^1	SIM^1	MB^2	ME^3	$RMSE^4$	R^5	IOA^6
NCP							
T2 (℃)	−0.46	−0.61	−0.15	0.78	1.04	0.97	0.98
RH (%)	53.30	55.86	2.56	3.40	4.30	0.97	0.97
WS (m s^{-1})	2.47	2.12	−0.35	0.47	0.64	0.76	0.75
WD (°)	196.89	184.58	−12.31	20.73	37.57	0.95	0.97
YRD							
T2 (℃)	6.55	6.45	−0.10	0.52	0.67	0.98	0.99
RH (%)	74.20	74.71	0.52	2.76	3.75	0.98	0.99
WS (m s^{-1})	2.39	2.13	−0.26	0.39	0.50	0.79	0.85
WD (°)	131.05	134.27	3.22	18.81	60.60	0.84	0.92

[1]OBS and SIM represent the mean observed and simulated values from 25 December 2017 to 2 January 2018, respectively.

[2]MB is the mean bias, $MB = \frac{1}{N}\sum(SIM_i - OBS_i)$; SIM_i and OBS_i are hourly observed and simulated values. N is the total number of hours.

[3]ME is the mean error, $ME = \frac{1}{N}\sum |SIM_i - OBS_i|$.

[4]RMSE is the root mean square error, $RMSE = \sqrt{\frac{1}{N}\sum(SIM_i - OBS_i)^2}$

[5]R is the correlation coefficient, $R = \frac{\sum[(SIM_i - \overline{SIM}) \times (OBS_i - \overline{OBS})]}{\sqrt{\sum(SIM_i - \overline{SIM})^2 \times \sum(OBS_i - \overline{OBS})^2}}$.

[6]IOA is the index of agreement, $IOA = 1 - \frac{\sum(SIM_i - OBS_i)^2}{\sum(|SIM_i - \overline{SIM}| + |OBS_i - \overline{OBS}|)^2}$.
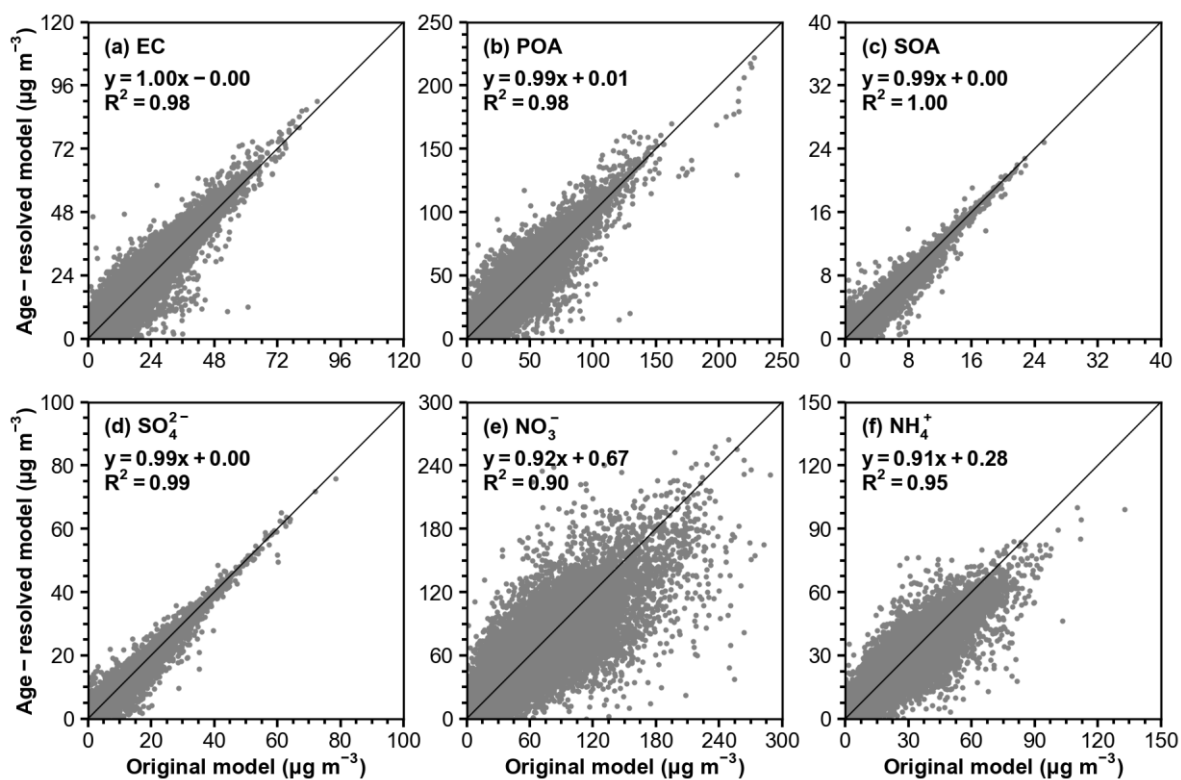
Figure S1. Comparison of EC, POA, SOA, SO_4^{2-}, NO_3^-, and NH_4^+ concentrations ($\mu g\ m^{-3}$) predicted by the age-resolved UCD/CIT model against the original UCD/CIT model for all grid cells within the model domain.
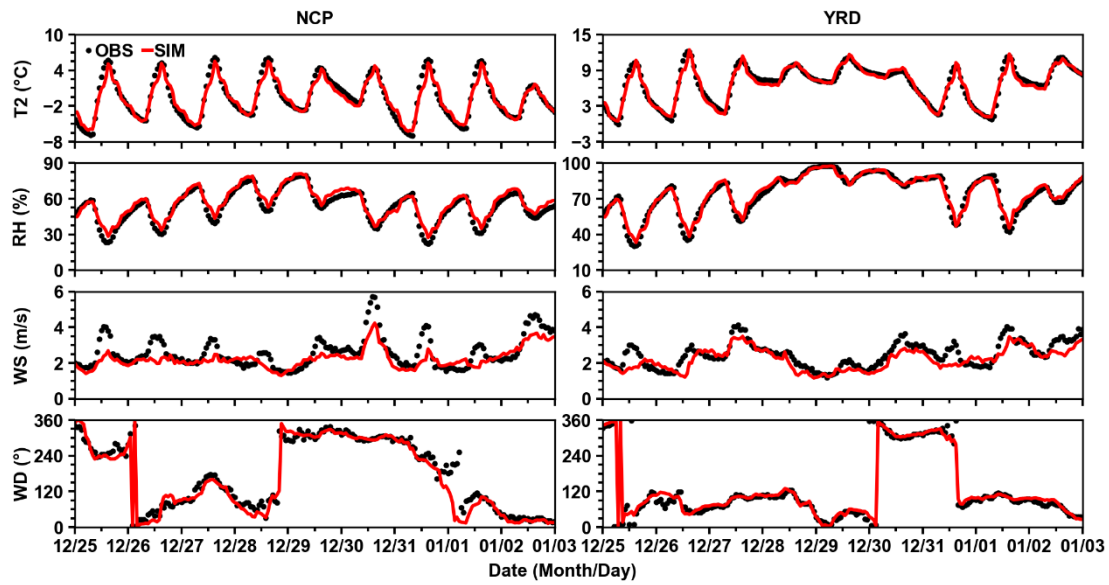
95

Figure S2. Time series of the observed (black dots) and simulated (red lines) hourly 2-m temperature (T2, ℃), 2-m relative humidity (RH, %), 10-m wind speed (WS, m s^{-1}), and 10-m wind direction (WD, °) at NCP and YRD during December 25, 2017 to January 2, 2018.
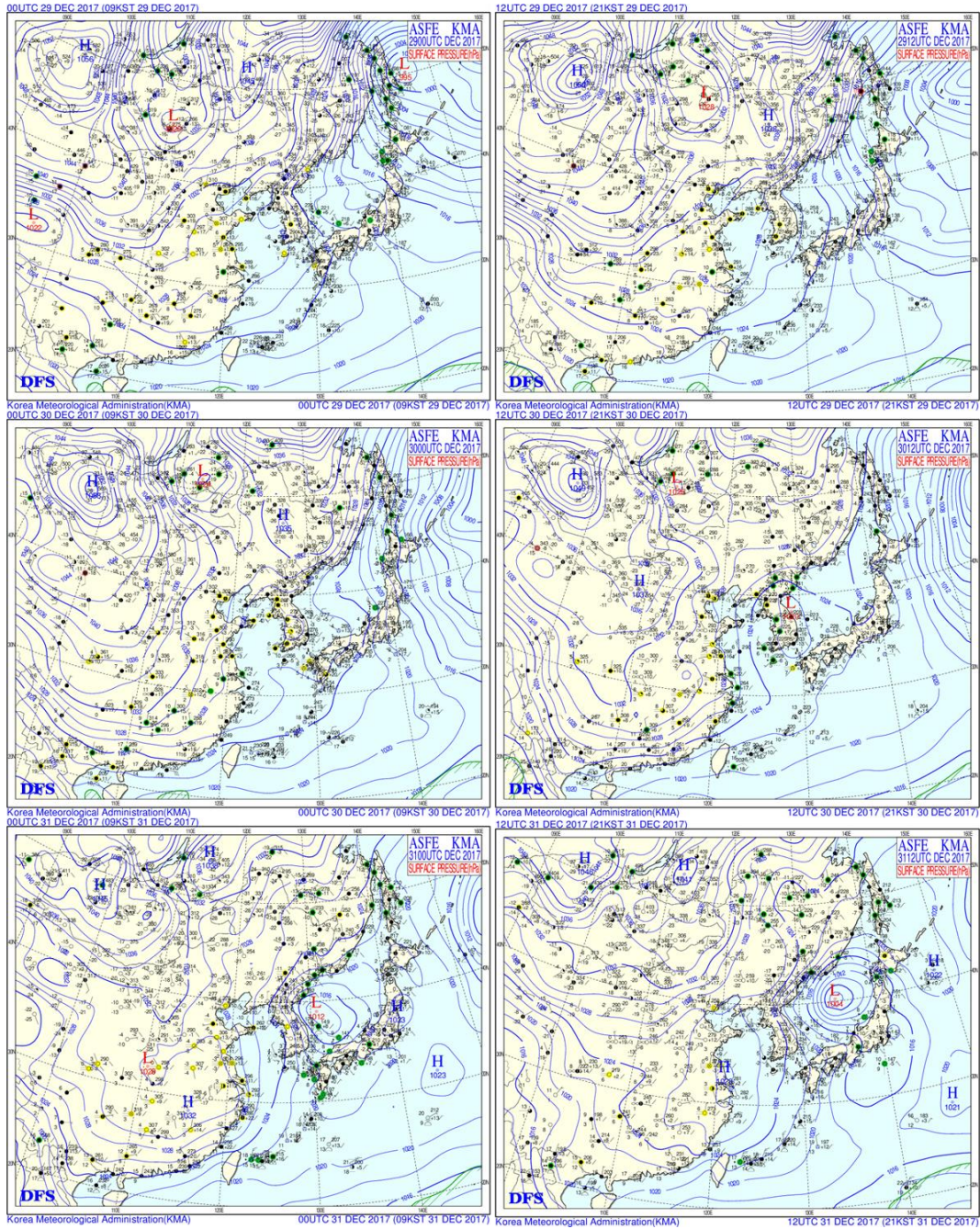
100

Figure S3. Surface weather pattern provided by the Korea Meteorological Administration (KMA; http://web.kma.go.kr/chn/weather/images/analysischart.jsp) over eastern Asia at 08:00, 20:00 LT 29–31 December 2017.

105
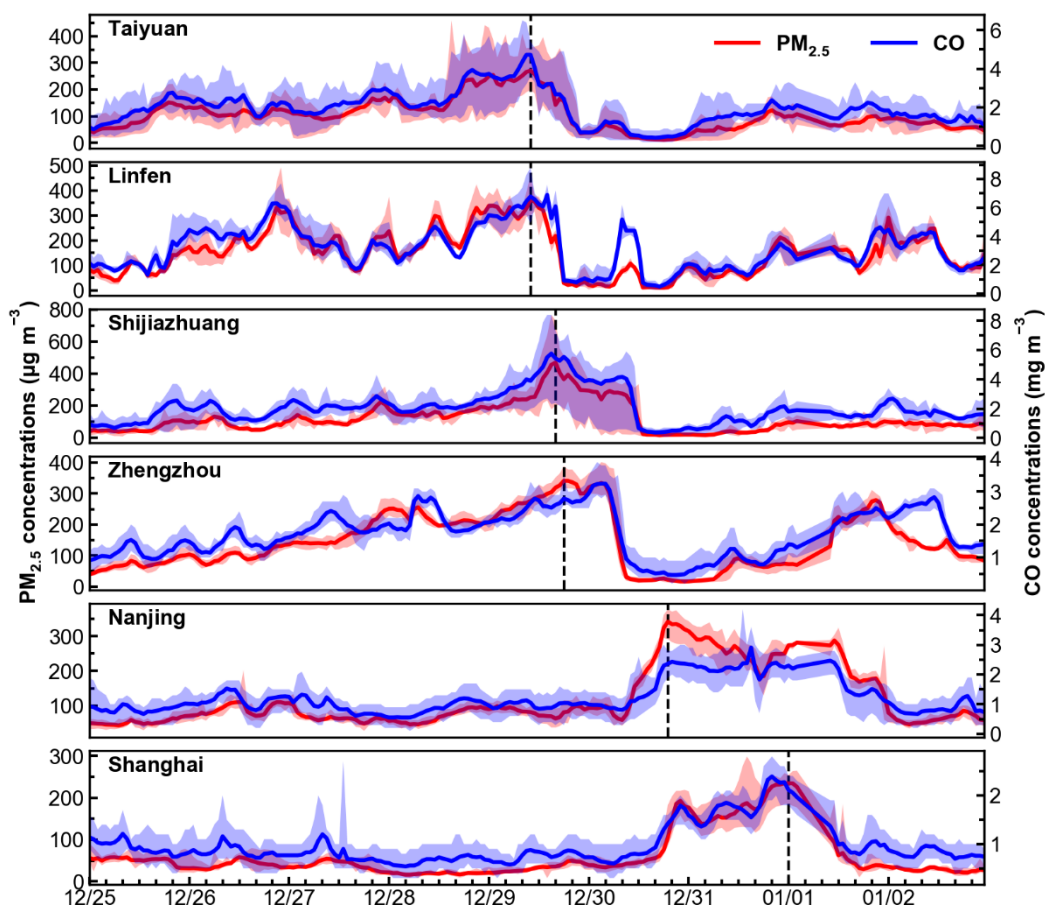
Figure S4. Time series of PM$_{2.5}$ (red lines) and CO (blue lines) concentrations in Taiyuan, Linfen, Shijiazhuang, Zhengzhou, Nanjing, and Shanghai. Shaded areas indicate the minimum–maximum range. Black dotted lines mark the peak PM$_{2.5}$ concentrations.

110
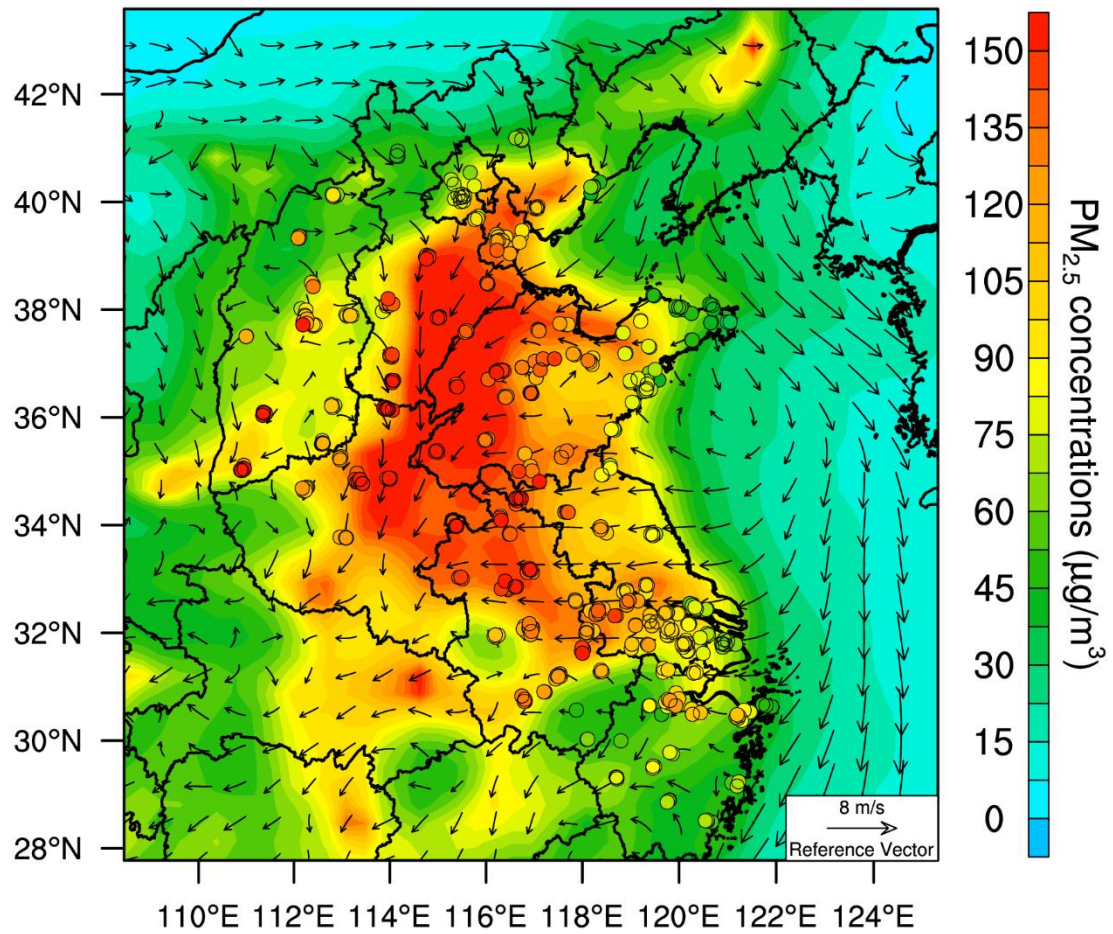
Figure S5. Spatial distribution of observed (circles) and simulated (shaded areas) episode-averaged PM$_{2.5}$ concentrations and the WRF-simulated 10-m wind fields over eastern China from December 25, 2017 to January 2, 2018.
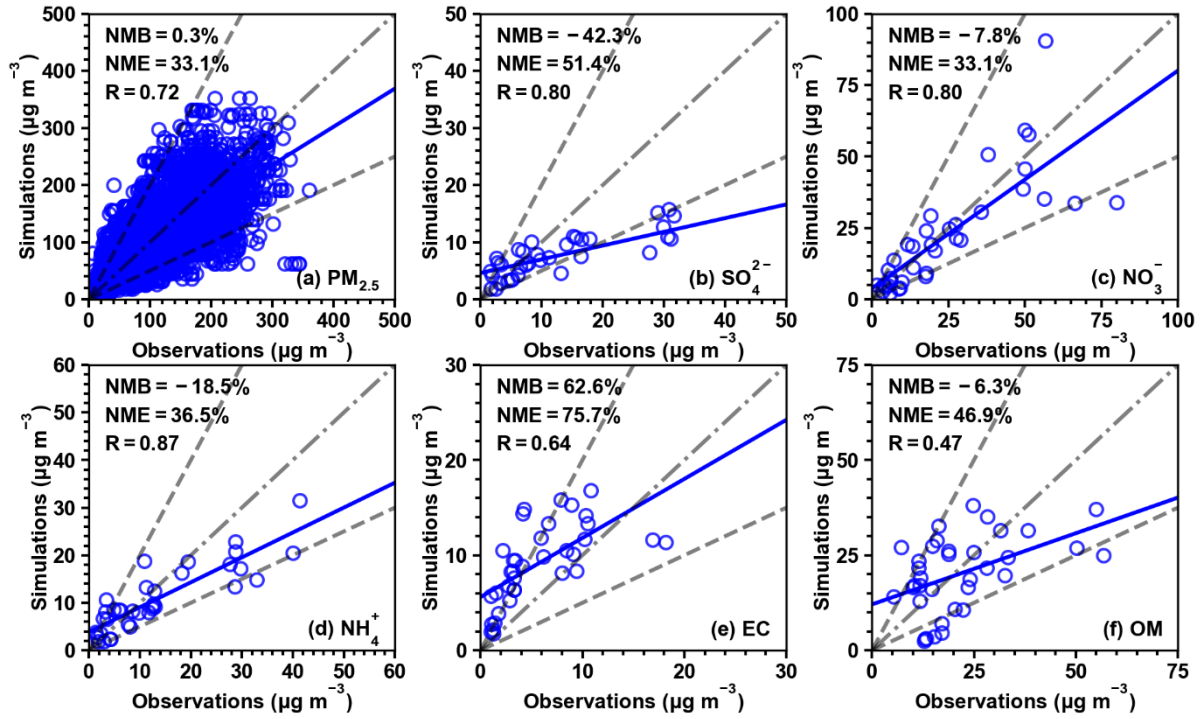
115

Figure S6. Scatter plots of simulated daily mean PM$_{2.5}$ in eastern China and its major chemical compositions (SO$_4^{2-}$, NO$_3^-$, NH$_4^+$, EC, and OM) in Beijing, Jinan, Nanjing, and Shanghai versus observed values from 25 December 2017 to 2 January 2018.
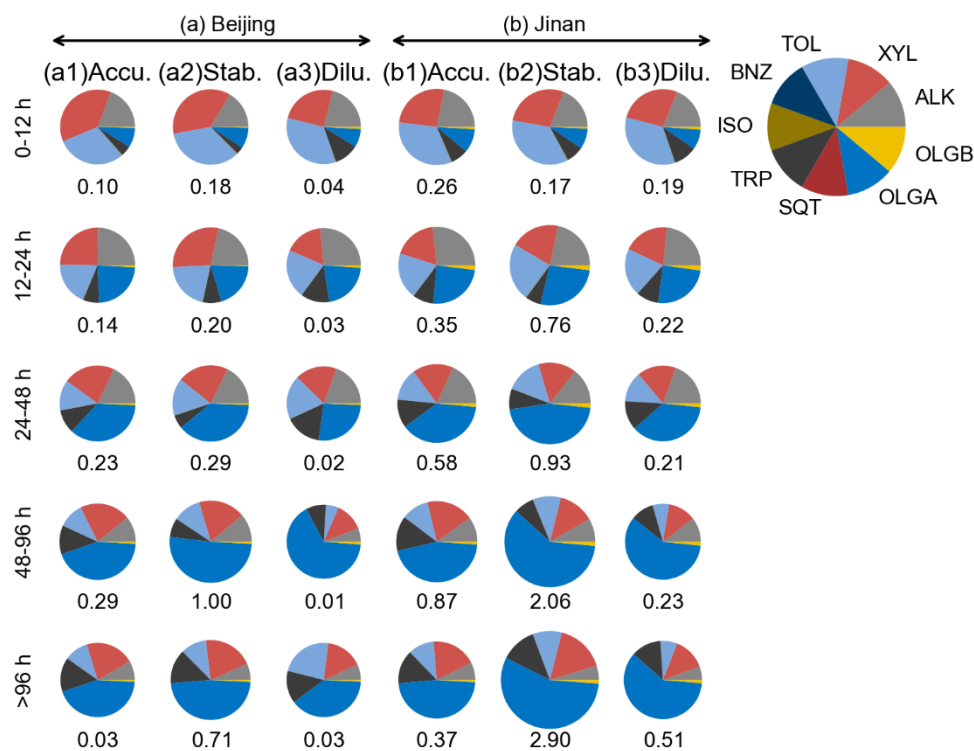
Figure S7. Fractional component contributions to SOA in different age bins in Beijing and Jinan. Accu., Stab., and Dilu. indicate the accumulation, stabilization, and dilution stage. ALK, XYL, TOL, BNZ, ISO, TRP, SQT, OLGA, and OLGB represent long-chain alkanes, xylene, toluene, benzene, isoprene, monoterpenes, sesquiterpenes, oligomers of anthropogenic SOA, and oligomers of biogenic SOA, respectively.
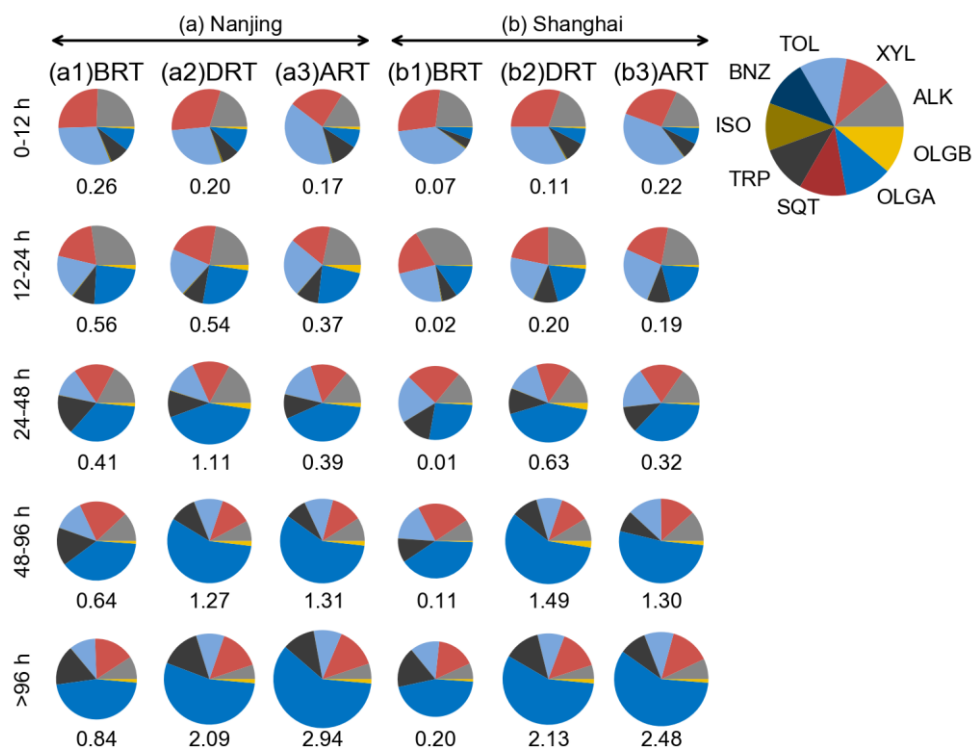
Figure S8. Fractional component contributions to SOA in different age bins in Nanjing and Shanghai. BRT, DRT, and ART indicate the period before, during, and after regional transport. ALK, XYL, TOL, BNZ, ISO, TRP, SQT, OLGA, and OLGB represent long-chain alkanes, xylene, toluene, benzene, isoprene, monoterpenes, sesquiterpenes, oligomers of anthropogenic SOA, and oligomers of biogenic SOA, respectively.
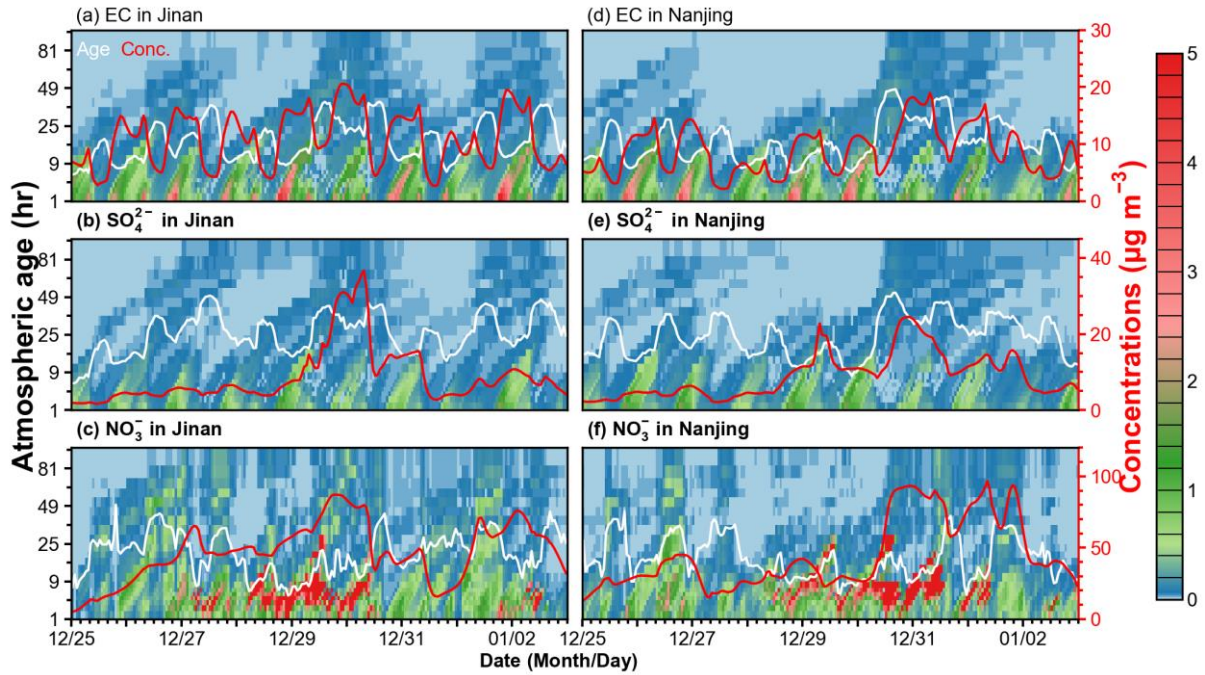
135 **Figure S9.** Hourly atmospheric age distribution of EC, SO_4^{2-}, and NO_3^- in Jinan and Nanjing during this haze episode. White lines represent the average atmospheric age, and red lines (right y-axis) indicate total mass concentrations. The results were combined from simulations with age-bin updating intervals of 1, 3, 6, 8, and 12 h.
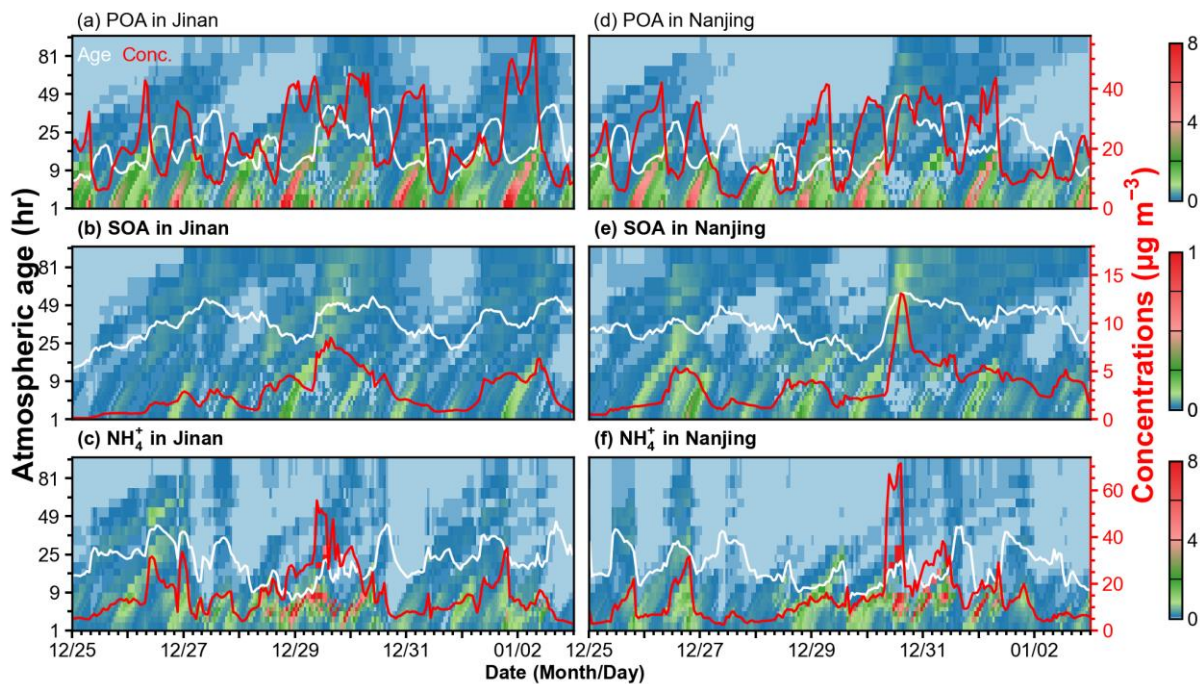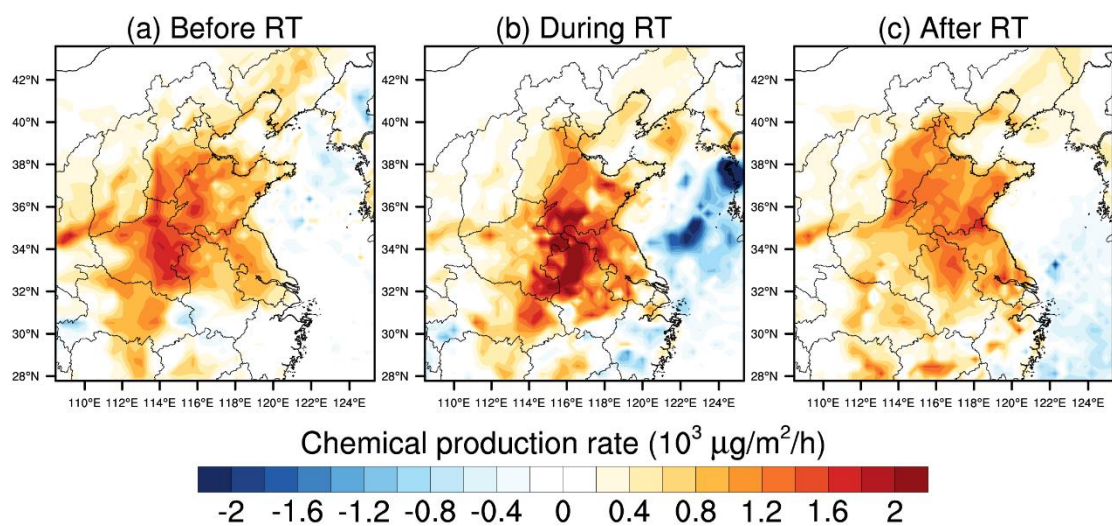
140

Figure S10. Hourly atmospheric age distribution of POA, SOA, and NH$_4^+$ in Jinan and Nanjing during this haze episode. White lines represent the average atmospheric age, and red lines (right y-axis) indicate total mass concentrations. The results were combined from simulations with age-bin updating intervals of 1, 3, 6, 8, and 12 h.
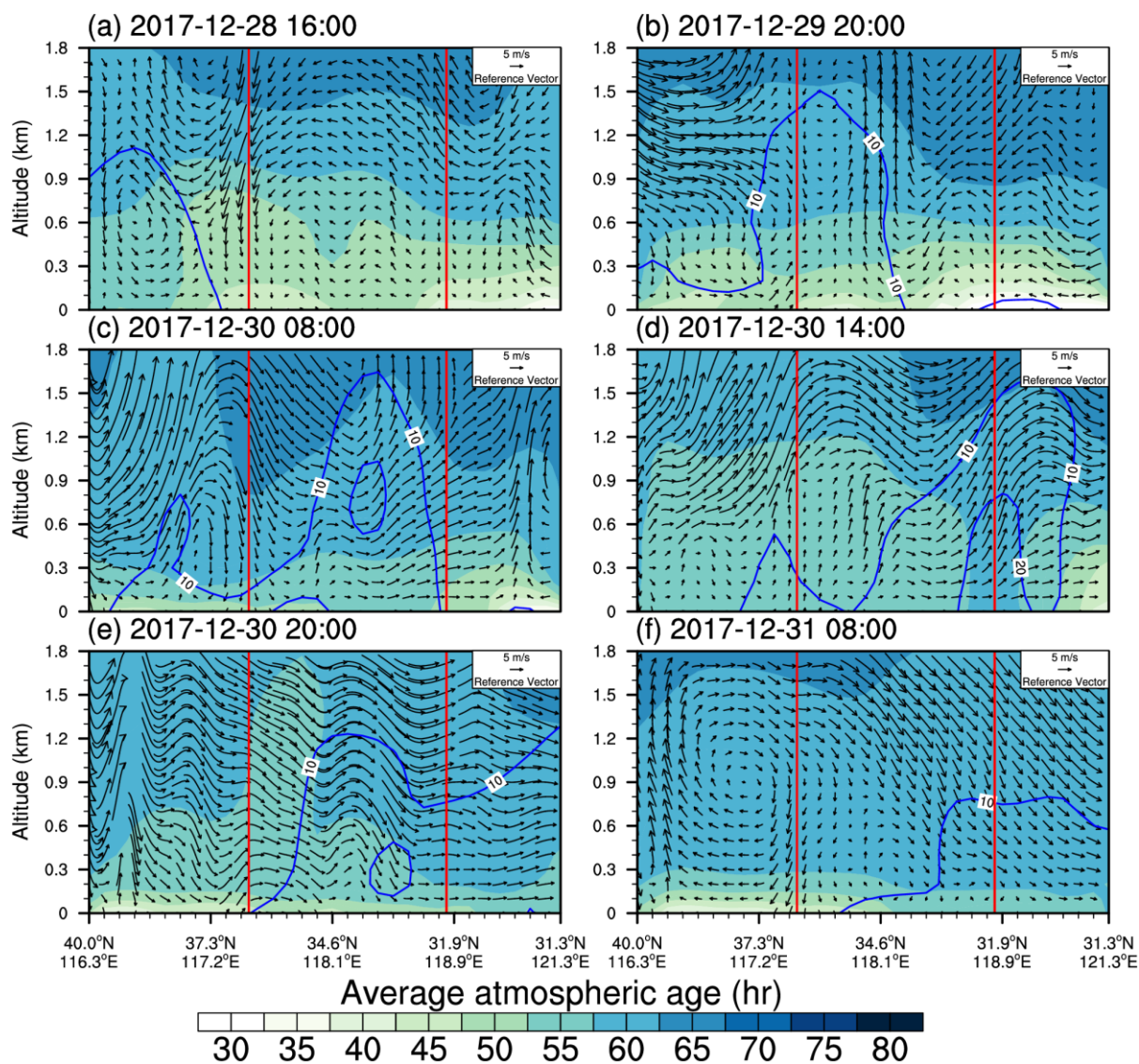
145

Figure S11. Spatial distribution of the averaged column chemical production rate of NO_3^- before, during, and after regional transport.
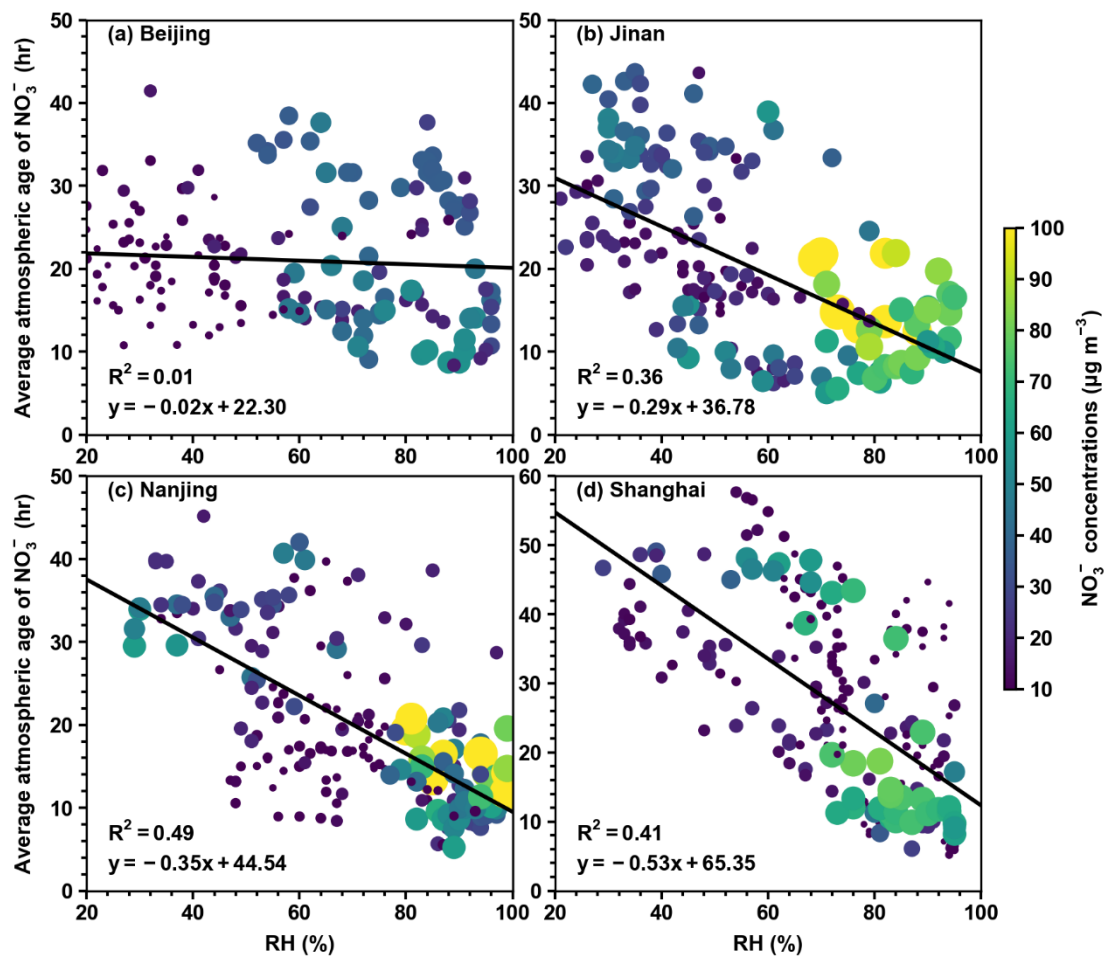
Figure S12. Average atmospheric age of NO_3^- as a function of RH in Beijing, Jinan, Nanjing and Shanghai.

150

Figure S13. Vertical cross section of the average atmospheric age (color contours; h) and concentrations (blue solid lines; µg m^{-3}) of SO$_4^{2-}$ along the transport route from Beijing to Shanghai (white solid line in **Figure 1**) at **(a)** 16:00 LT 28 December, **(b)** 20:00 LT 29 December, **(c–e)** 08:00, 14:00, 20:00 LT 30 December, and **(f)** 08:00 LT 31 December 2017. Note that the vertical wind speed was multiplied by 500 for the illustration of vertical circulations. The location of Jinan and Nanjing are marked as red solid lines.

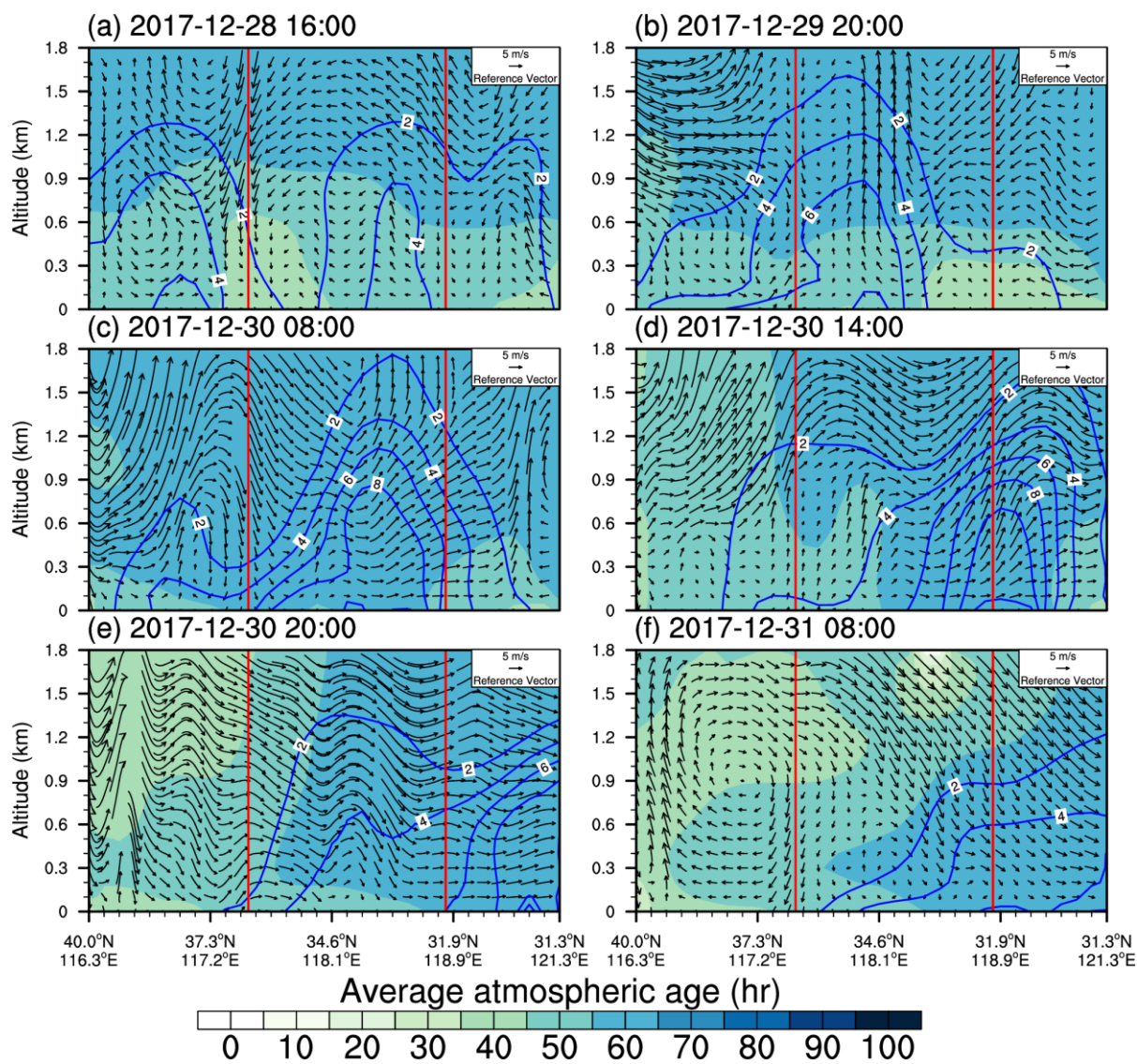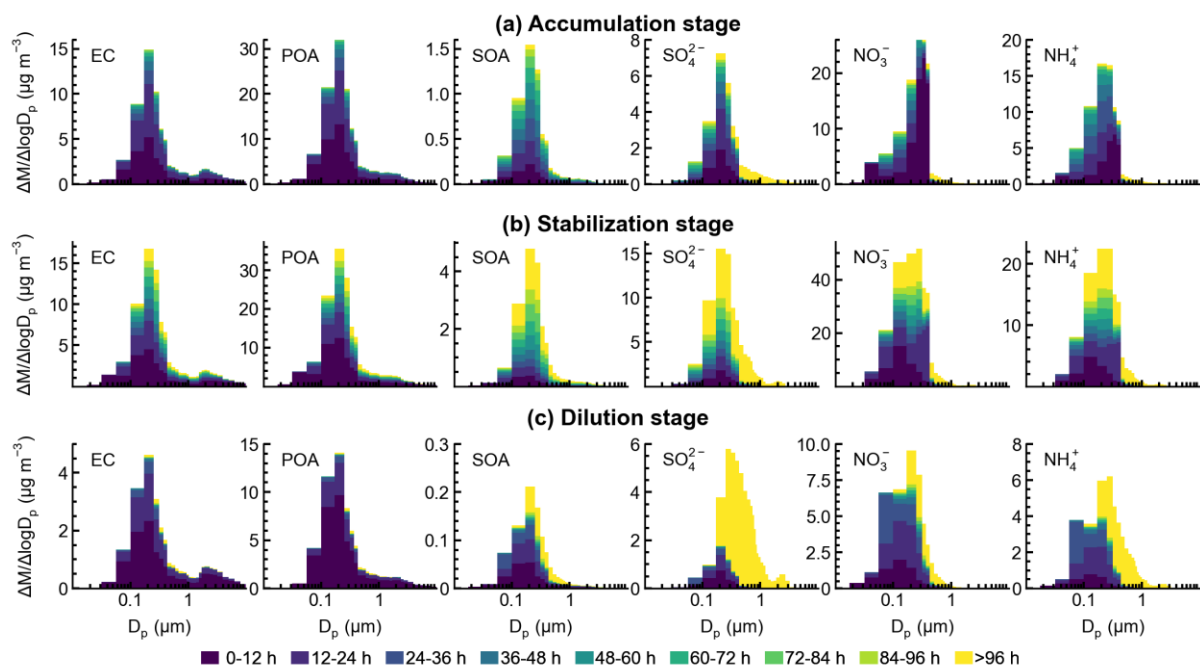**Figure S14.** Same as **Figure S13** but for SOA.

165

Figure S15. The size distribution of EC, POA, SOA, SO_4^{2-}, NO_3^-, and NH_4^+ in Beijing during (a) accumulation stage, (b) stabilization stage, and (c) dilution stage.